

Damage measurements after creep tests on samples of HP-40 alloys modified with a low level addition of Nb

R.Voicu¹, J. Lacaze¹, E. Andrieu¹, D.Poquillon¹, J. Furtado²

¹*CIRIMAT, Toulouse, France;* ²*Air Liquide –C.R.C.D, Jouy-en-Josas, France*

Keywords: creep damage, austenitic stainless steels

Abstract

Centrifugally cast tubes of heat resisting alloys are widely used in reformers and other high temperature chemical industries. In the present paper, the creep behavior of two different HP-40 alloys modified with a low level addition of Nb is investigated. The study focuses on damage localization and on damage quantification. Creep tests are carried out at 980, 1030 and 1050°C with different stress levels, in the range of 20 to 50 MPa. A qualitative and quantitative analysis of creep damage is carried out that needed a special procedure which is detailed. As for the results, emphasis is put on the effect of the stress level and on the difference between the two alloys.

1. Introduction

HP-40 1% Nb centrifugally cast reformer tubes are the main components of a hydrogen production plant. The tubes have inside diameter of 60 to 120 mm and are 10 to 14 m long. They are designed for a nominal life of 100,000 h in service conditions, typically 980°C with an internal pressure of 10 to 40 bar [1-4]. However, reformer tube life is limited by creep, driven by a combination of internal pressure and through-wall thermal stresses generated during process and by shut-down and start-up cycles. Over the past two decades, many researches have been devoted to damage analysis of failed tubes [2, 5-7], and some works focused on the assessment of remaining life [4, 6, 8].

The present paper gives results obtained on two different HP-40 alloys (modified with a low level addition of Nb) during laboratory creep tests and focuses on damage characterization and on damage quantification. An important aim of this study was to localize the damage, namely to settle if it is located only at grain boundaries or if it can be also intra-granular. Set-up of an appropriate methodology was necessary in order to answer this question. A systematic quantification of damage has been performed on samples after creep tests at high and low stress levels, on both alloys.

¹ D. Poquillon Tel: 33 562885662 Dominique.Poquillon@ensiacet.fr

2. Experimental methods

The specimens tested during this study were taken from two as-cast tubes, labeled A and B, made of HP-40 alloy containing 1 wt. % Nb. The nominal composition of the alloy and the chemical analysis of the materials are given in Table 1. As described previously [10], the as-cast microstructure of both alloys consists in a dendritic matrix of γ austenite and an eutectic network of Nb-rich MC and Cr-rich M_7C_3 carbides. Section of tube B showed only columnar grains while tube A has columnar grains in its outer part and equiaxe grains in its inner part.

	Fe	Ni	Cr	Nb	Si	C
Nominal composition	balance	33-37	24-28	1.0	<2	0.35-0.75
Material A	balance	32.6	25.5	1.0	1.5	0.8
Material B	balance	34.9	26.0	1.4	0.6	0.6

Table 1 : Nominal composition (wt. %) of HP-40 alloys modified with Nb [9] and results of GDMS analysis of materials A and B.

The specimens for mechanical tests were machined from the tube as shown in Fig. 1a so that the length of the samples is parallel to the tube axis. Accordingly, the primary dendrite trunks are perpendicular to the direction of the principal stress applied. Fig. 1b is a schematic of the creep samples that have a thickness of 2 mm, so that the gage section is 8 mm². Before testing, the specimens were mechanically polished (down to 3 μ m diamond paste) and their dimensions were measured using an optical microscope.

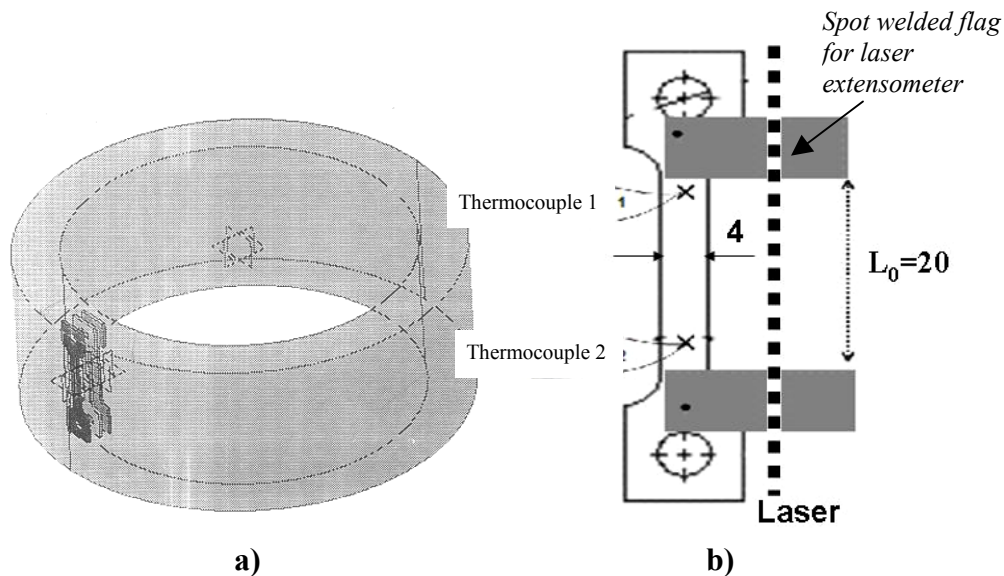


Figure 1: a) Sampling of the specimens in the tube thickness; b) schematic of a creep specimen (dimensions are in mm), thickness is 2 mm. The location of the thermocouples and of the flags used for laser extensometer are also indicated.

Tests were performed on a creep testing device equipped with an x20 balancing arm. They were carried out under a slight overpressure (0.1 bar) of argon in order to prevent the material from oxidizing. Two K thermocouples spot welded on the sample heads were used for temperature control. For all experiments, the heating rate to the target temperature was set to 50 °C.min⁻¹ and the maximum temperature difference observed along the 20 mm gage length was 5 °C. After heating, a ten minutes dwell time was applied for temperature homogenization. A laser extensometer was used to measure the distance between the two flags spot welded on the heads of the sample (Fig. 1b), so that the deformation was measured during creep tests without contact.

Creep conditions	Material	Test duration (h)	$\dot{\epsilon}$ (s ⁻¹)	Creep strain (%)	Damage D _{min} (%)	Damage D _{max} (%)	Average damage (%)
20 MPa 980°C	A	11	9.5x10 ⁻⁹	0.06	0.19	0.86	0.32
	A _{bulk}	146	3.8x10 ⁻⁸	17	0.16	1.57	0.7
	A _{outer surface}				1.2	32	6.8
	A (4x5mm ²)	426.5	2.4x10 ⁻⁹	0.5	0.06	1.78	0.33
	B	9.7	7x10 ⁻⁹	0.04	0.09	0.22	0.16
50 MPa 980°C	A	1.4	2x10 ⁻⁵	24	0.025	31.4	3.88
	B	9	10 ⁻⁶	15.7	0.05	32.5	1.85
50 MPa 1030°C	B	2.25	10 ⁻⁵	23	0.03	7.5	1
50 MPa 1050°C	A	0.5	5x10 ⁻⁵	23	0.035	22	1.78
	B	1.97	1.25x10 ⁻⁵	21	0.08	5.8	1.55

Table 2: List of the crept samples used for damage quantification. For samples tested to rupture, test duration, creep strain and damage levels are indicated with bold font, while normal font is used for interrupted tests. The minimal, maximal and average damage quantified are reported in the three last columns.

Creep tests have been performed at 980, 1030 and 1050°C with various stress levels, in the range 20 to 50 MPa. Some tests were performed until rupture, while others were stopped during the secondary creep stage in order to study damage initiation. Table 2 summarizes the tests conditions and creep parameters (test duration, final creep strain, minimum strain rate $\dot{\epsilon}$) for those samples on which damage was characterized.

After creep, a qualitative analysis was done in order to localize the cavities and cracks in the material. As only optical micrography allows observing the grains (after appropriate etching detailed below) and only SEM observations show cracks and cavities, a procedure was settled to visualize both microstructure and damage microstructure. As illustrated in Fig. 2, the correspondence of optical and SEM images was carried out using macro-cracks which can be observed by both

techniques.

For this damage analysis, specimens were first mirror polished (up to ¼ diamond paste) and then cleaned (ultrasonic bath cleaning during 5 minutes in a alcohol and water mixture) and dried. Then, they were electrolytically polished (2 V, 10 s, 10% perchloric acid and 90% ethanol) in order to uncork and reveal cracks and cavities for SEM observations. After that step, the specimens were etched with a mixture made of 48 g NH₄F-HF, 800 ml H₂O and 400 ml HCl in order to reveal grains (optical microscopy observations). At the end, a mapping of cracks and cavities (SEM observations) in relation with grain boundaries and large cracks (optical microscopy observations) was established.

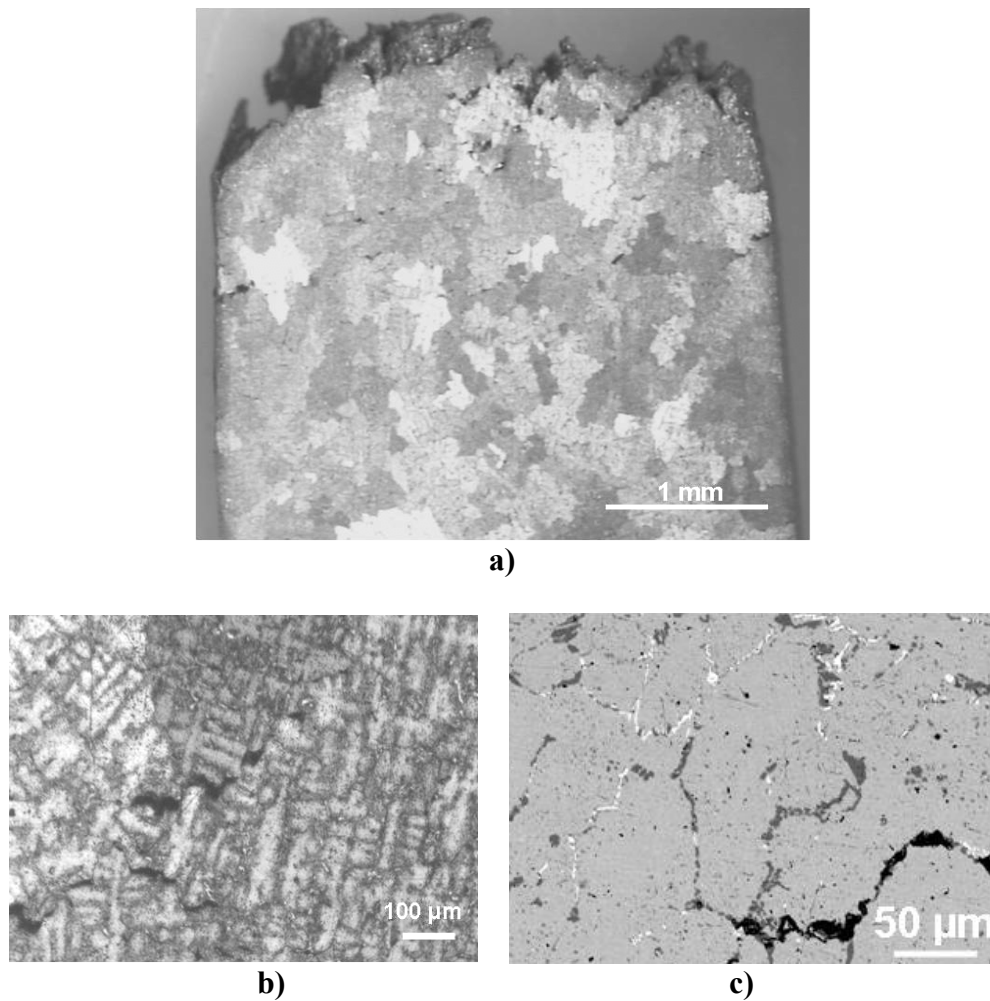


Figure 2: Micrographs from a specimen after 146 h of creep at 980°C under 20 MPa. a) optical image showing localization of damage (cracks) at grain boundaries; b) zoom on a); c) SEM image (backscattered electrons) showing the cracks localized at interdendritic areas.

Furthermore, during SEM observations, backscattered electrons micrographs were also taken at appropriate magnification for damage quantification. These images were afterwards thresholded and analyzed with Scion software as illustrated in

Fig. 3 in order to obtain the surface fraction of damage, D (%). This damage quantification was carried out along the median axis of the gage length of the specimens, at different distances from the fracture surface. The average damage value given in Table 2 is the average of the results obtained on 10 pictures taken along the gage length. In order to have some indication of the possible localization of damage, the minimal and the maximal values have been also reported in Table 2.

For one sample of A material, the procedure for damage evaluation was repeated in the core, thus allowing comparing values from the surface and the bulk of the sample in that case. The corresponding results are also listed in Table 2.

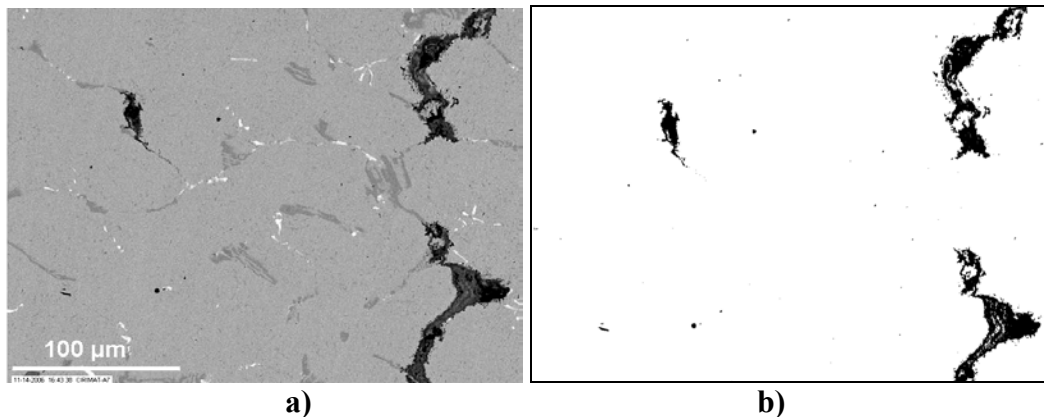


Figure 3: a) Backscattered electron SEM image of a specimen crept under 50 MPa at 1050°C; b) binary image of a) giving the surface fraction of cavities.

3. Results

Creep tests performed at 980°C at different stress levels showed that the lower the applied stress is, the higher the creep life and the lower the strain to fracture are. Examples are given in Fig. 4a in the case of material A. For longer creep tests, i.e. at lower stress values, aging of the microstructure appeared to be a significant factor affecting damage characteristics and creep life. Fig. 4b shows an example of records that illustrates the fact that the creep resistance of material B was found to be much better than the one of the material A. First damage observations performed on interrupted test samples showed that creep cavities appear during the secondary creep stage, and that they are localized at the carbide/ γ matrix interfaces as illustrated in Fig. 2c.

Creep specimens tested at high stress level (40 and 50 MPa) always failed with a significant necking of the gage. Damage (cavities and cracks) was evidenced and localized near the fracture surface as shown by the example in Fig. 5. These damage observations are in agreement with the recorded mechanical behavior that shows a very short tertiary domain. Plastic instability induces strain localization and seems to be the main reason for the fracture for both alloys in that case.

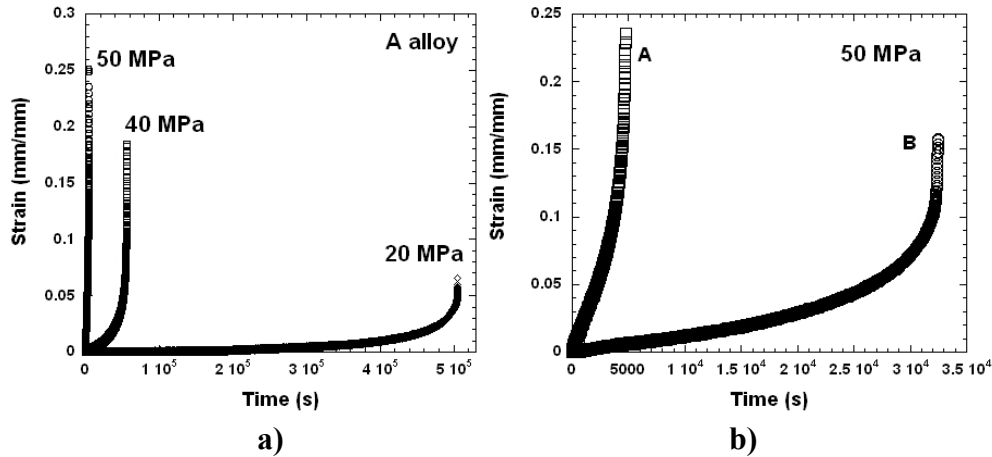


Figure 4: Creep strain versus time curves for experiments at 980°C. a) effect of stress level in the case of A as-cast alloy; b) comparison of A and B materials crept under 50 MPa.

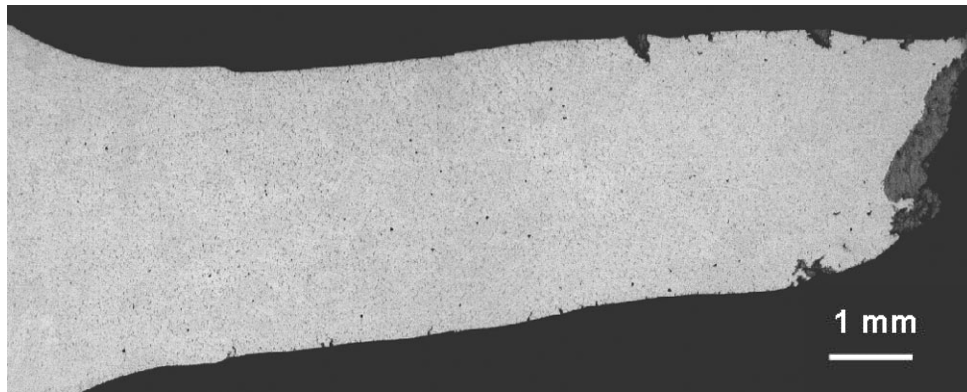


Figure 5: SEM images of gage the A specimen after creep at 980°C in argon) under 50 MPa showing necking and damage localization near rupture.

For specimen tested at 20 MPa, no marked necking was observed as seen in Fig. 6. Damage, i.e. cavities and cracks, were located in a large zone even far from the fracture surface. The creep cracks observed were mainly located at grain boundaries, but closer observations showed the presence of cavities within the grains in the interdendritic areas. Fracture appears to be linked to the macro-damage (cracks) but this result would have to be confirmed on other specimens tested at similar low stress levels. It is worth stressing that, for all samples, the cracks observed appear essentially perpendicular to the direction of the applied stress, though the rupture is interdendritic and presents a ductile appearance.

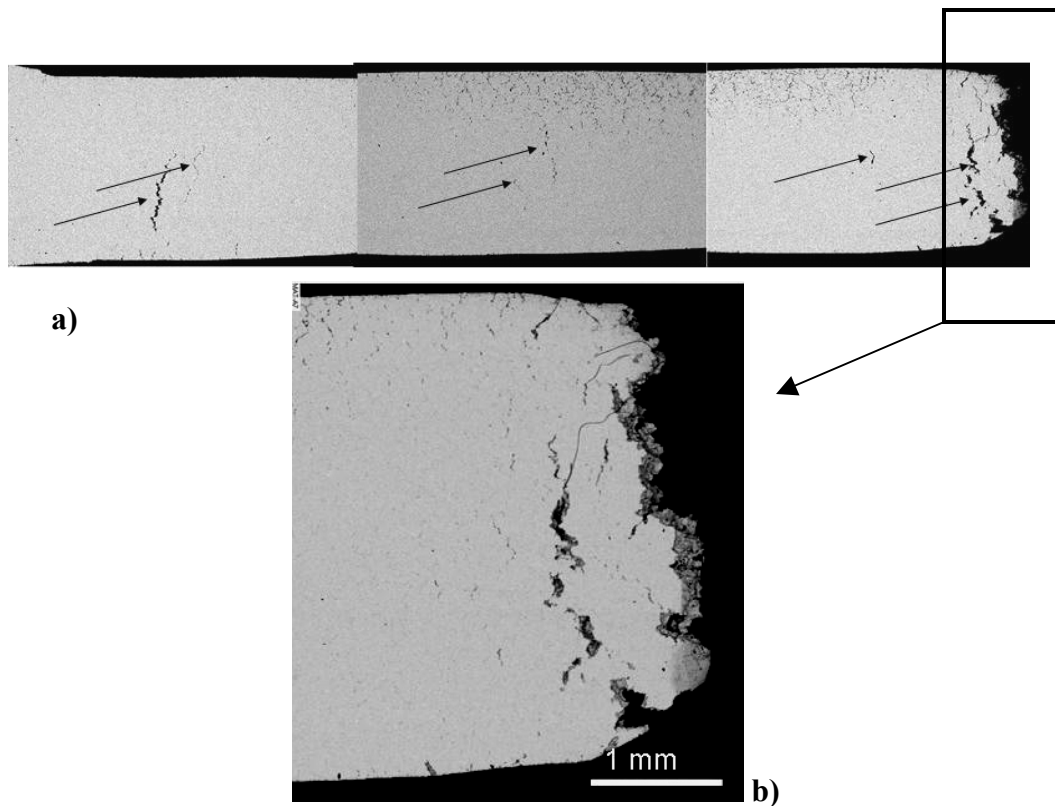


Figure 6: a) SEM image of the gage of a sample crept at 980°C under 20 MPa showing damage distribution all along the gage length (arrows); b) zoom on a)

In the case of low stress crept samples, the quantification of damage shows that not only damage has expended all along the gage length but also that its minimal level is much higher than for samples tested at high stress levels (Table 2). For short time creep tests at 50 MPa, the maximal value of damage was also quite high but the average damage remained small (1 to 3.9 %) because the damage value was strongly reduced far from the fracture surface. At lower stress and for longer creep duration, the final creep strain was lower than for higher stress values but the minimal damage values were higher. These observations are illustrated by the graphs in Fig. 7 where the values of D have been plotted for A samples crept at 980°C under 50 MPa (Fig. 7a) and 20 MPa (Fig. 7b). For the former sample, a quantification of necking was also carried out that consisted in measuring the evolution of the surface section S all along the gage length of the specimen. The corresponding change of the ratio S/S_0 , where S_0 is the initial section size, has also been reported in Fig. 7a. The strong necking of the sample is thus stressed and easily correlated to localization of the damage. By comparing Fig. 7a with Fig. 7b, it is seen that the damage is no more localized as the stress level is decreased while its value has increased to 6.9 %. This damage distribution is illustrated by the micrograph in Fig. 6a.

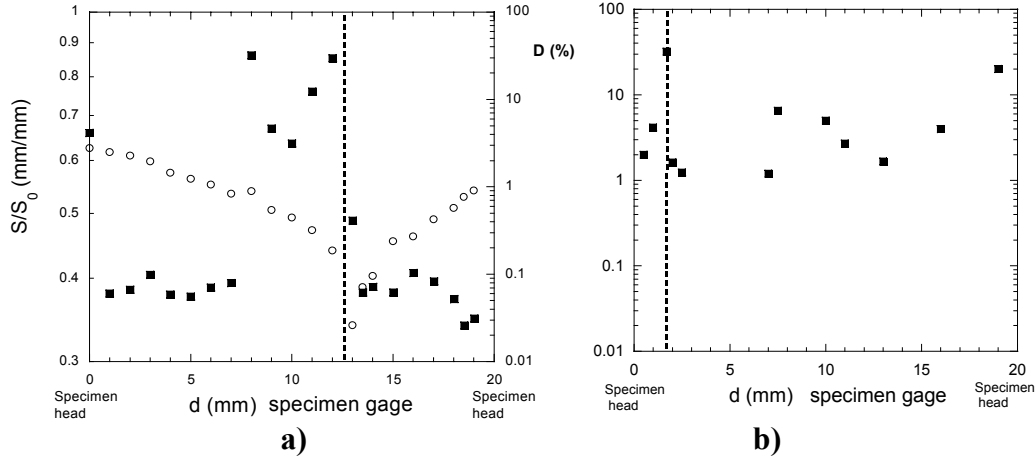


Figure 7: Damage distribution (full symbols) and section evolution (empty symbols) measured on A material after creep at 980°C under 50 MPa for 1.4 h (a) and under 20 MPa for 146 h (b). The interrupted line in each graph locates the observed fracture zone.

4. Discussion:

Observations and damage quantification confirmed previous results [10] where a change of the creep damage mechanisms was observed on both alloys A and B when passing from high to low stress levels. Furthermore, comparing the two alloys, creep strain levels at rupture are similar, but damage is systematically slightly higher on alloy A which exhibits always shorter creep life than the B one. Creep tests performed at different temperatures on A and B alloys showed that for A material the damage as well as the strain ratios are comparable when passing from the service temperature (980°C) to a higher one (1050°C). In the case of alloy B, a slight increase of both strain and damage levels are observed when rising the temperature. This has been tentatively related to a difference in aging kinetics of the microstructure [11].

In a parallel study [12], the effect of the specimen gage section was underlined. The characteristic size of the dendrites, as given by the average size of their secondary arms, is quite large at about 50 μm when compared to the 2 mm^2 sample section used previously [10]. It was thus decided to use larger samples with 8 mm^2 gage section as in the present study so as to get samples with a volume being more representative of the bulk material. In the present work, a specimen with an even larger gage section at 4x5 mm^2 was machined from material A. This sample was tested at 980°C under 20 MPa, and showed a slower minimal creep strain rate than samples with smaller section size (Table 2). However, it was found that the damage undergone by the material is very similar in both cases, so that section size of 4x2 mm^2 is large enough with respect to the characteristic dimensions of the microstructure for damage evaluation.

A literature review on ex-service reformer tubes shows that the damage

distribution can be homogeneous with equidistant radial cracks [8], and related to low internal stress and moderate and almost homogeneous temperature (<900°C) of the tube during service. No thickness tube deformation was observed in that case [8]. Similarly, the present creep damage results showed the damage to be distributed all along the gage length, without necking near the fracture zone, for specimens tested isothermally at low stress level. However, most of the works on ex-service tubes have reported inhomogeneous damage distributions [3, 4, 7]. Le May et al. [3] proposed a damage classification based on the Neubauer and Wedel approach[13] with five levels of damage. Indeed these studies have underlined an important damage ratio (as cracks) near the fracture zone and the presence of cavities through the rest of the tube thickness, often associated also with a significant strain level [14]. The present study shows that when increasing the applied stress, strain and damage localize near the fracture zone. For in-service conditions, damage induces a local increase of stress, of temperature (because of the process) and of creep strain. This enhancement has a detrimental effect on life duration of the tube. The above remarks suggest that thermo-mechanical local gradients are responsible for damage enhancement and its inhomogeneous distribution.

5. Conclusion

The results of the present study allowed to locate macro-damage as occurring mainly at grain boundaries as cracks. However, closer observation of samples obtained through interrupted creep tests showed the presence of an intragranular damage (cavities) localized at the carbides/ γ matrix interfaces, i.e. in interdendritic areas within the grains. Furthermore, it has been stressed that the damage is distributed all along the gage length for low stress levels, while rather localized near rupture for high levels. Interestingly enough, it was showed that the damage appears during the secondary creep stage and develops mainly perpendicularly to the direction of the applied stress leading to an interdendritic fracture mechanism. When comparing the two alloys, material B exhibits always a higher creep life than material A, with the latter showing an increased creep damage level than the former. Slight composition differences between these alloys may play a major role on microstructure aging and mechanical properties. This could possibly also explain the slight difference in the creep behavior of the two alloys that was observed when the test temperature is increased from 980 to 1050°C.

References

- [1] K.S. Guan, F. Xu, Z.W. Wang, H. Xu, Failure analysis of hot corrosion of weldments in ethylene cracking tubes, *Eng. Fail. Anal.* 12 (2005) 1-12
- [2] Refineries C.o.H.-T.T.i.P. API Recommended Practice 530, 3rd edn., American Petroleum Institute 1988, Washington DC.
- [3] I. Le May, T.L. De Silveira, C.H. Vianna, Criteria for the evaluation of damage and remaining life in reformer furnace tubes, *Int. J. Press. Vessels Pip.* 66

(1996) 233-241

[4] A.K. Ray, K.S. Amarendra, N.T. Yogendra, J. Swaminathan, G. Das, S. Chaudhuri, R. Singh, Analysis of failed reformer tubes, Eng. Fail. Anal. 10 (2003) 351-362

[5] S.K. Bhaumik, R. Rangaraju, M.A. Parameswara, T.A. Bhaskaran, M.A. Venkataswamy, A.C. Raghuram, R.V. Krishnan, Failure of reformer tube of an ammonia plant, Eng. Fail. Anal. 9 (2002) 553-561

[6] D. Jakobi, R. Gommans, Typical failures in pyrolysis coils for ethylene cracking, Mater. Corros. 54 (2003) 881-886

[7] M.H. Shariat, A.H. Faraji, A. Ashraf-Riahy, M.M. Alipour, In advances creep failure of HP modified Reformer Tubes in an Ammonia Plant, Corrosion Science in the 21st century 6 (2003) H012

[8] J.M. Brear, J.M. Church, D.R. Humphrey, M.S. Zanjani, Life assessment of steam reformer radiant catalyst tubes - the use of damage propagation methods, Int. J. Press. Vessels Pip. 78 (2001) 985-994

[9] ASM Handbook, Properties and Selection: Irons, Steels and High-Performance Alloys 1, ASM International, (1990) 910

[10] R. Voicu, J. Lacaze, E. Andrieu, D. Poquillon, J. Furtado, Creep behaviour of HP-40 alloy modified with a low level addition of Nb, proceedings of the 2nd International ECCO Conference (2009)

[11] R. Voicu, PhD thesis, Université de Toulouse, November 2008

[12] R. Voicu, J. Lacaze, E. Andrieu, D. Poquillon, J. Furtado, Creep and tensile behaviour of austenitic Fe-Cr-Ni stainless steels, Mater. Sci. Eng., A, in press

[13] B. Neubauer, V. Wedel, Rest life estimation of creeping components by means of replicas, ASME international Conference on Advances in Life Prediction Methods (1983), New York

[14] K. Guan, H. Xu, Z. Wang, Quantitative study of creep area of HP40 furnace tubes, Nucl. Eng. Des. 235 (2005) 1447-1456